Research Square

Preprints are preliminary reports that have not undergone peer review.
They should not be considered conclusive, used to inform clinical practice,
or referenced by the media as validated information.

Arithmetic blindness and its removal in energy-transfer channels

Ahmet Faruk Arapoğlu

ahmetarapoglu@gmail.com

Research Article

Keywords: quantum observability, energy transfer, quantum channels, frequency degeneracy, correlations, quantum thermodynamics

Posted Date: November 3rd, 2026

DOI: https://doi.org/10.21203/rs.3.rs-11575647/v1

License: This work is licensed under a Creative Commons Attribution 4.0 International License.
Read Full License

Additional Declarations: No competing interests reported.

Arithmetic blindness and its removal in energy-transfer channels

Ahmet Faruk Arapoğlu[1*]

[1]Independent Researcher, Istanbul, Türkiye.
ORCID: 0009-0005-9374-3368.

Corresponding author(s). E-mail(s): ahmetarapoglu@gmail.com;

Abstract

An energy-conserving receiver can fail to distinguish sources with identical local states and ergotropy. Starting from the frequency-graph description of transpose-pair contrast, we study how interaction design changes this blindness. For general symmetric amplitudes, we classify dark-transition bias and derive a sharp stability threshold for the standard Hamiltonian. An explicit bounded dressing restores exact identifiability on every finite alphabet. Finite-time sensitivity, calibration error and equal-peak comparisons then distinguish exact recovery from useful measurement. Exact arithmetic and full Hamiltonian calculations support a finite-shot discrimination protocol, while multiplication-table structure supplies the reference blind model.

Keywords: quantum observability, energy transfer, quantum channels, frequency degeneracy, correlations, quantum thermodynamics

1 What an interaction fails to see

Two sources can look the same to every measurement of either mode alone and still carry different joint records. Even a receiver that exchanges energy with them may never notice the difference. In the model studied here, this failure has a concrete cause: distinct occupation transitions are assigned the same Rabi frequency. Their contributions cancel at every time. Waiting longer cannot recover a distinction that has already vanished from the receiver's response.

The thermodynamic role of correlations is well established. Correlations can store extractable work, affect heat exchange, and change the transport of ergotropy [1–3]. Ergotropy itself concerns the energy extractable by an unrestricted unitary on a specified system [4]. It does not specify what one fixed interaction can read. Our question is therefore narrower: when two sources have equal local states, spectrum, mean energy and ergotropy, which of their remaining differences reach a particular receiver?

The general language for this question is observability. Quantum observability and dynamical tomography characterize equivalence classes of states that produce identical measurement records [5–8]. Restricted measurements can hide distinctions that a global measurement readily resolves; quantum data hiding provides a different, well-developed setting for that phenomenon [9, 10]. We do not infer that hidden information or nonlinear atom–field coupling is new. Intensity-dependent and two-mode Raman models already provide exact examples of occupation-dependent dynamics [11–13].

The source is a number-diagonal distribution P over two bosonic modes. We compare it with its transpose P^{T} and require equal row and column marginals. The difference $J = P - P^{\mathsf{T}}$ is then a circulation on the occupation alphabet. The receiver applies a second boundary map, now on a graph whose vertices are Rabi frequencies. A source difference is invisible exactly when it has zero boundary in both graphs. For the standard exchange amplitude, repeated products in an integer multiplication table create an asymptotically dominant blind subspace. A cubic-algebraic dressing separates the relevant pairs; a bounded version gives the same exact identifiability without an energy spectrum extending to minus infinity.

We study general symmetric amplitudes, dark-transition bias and bounded observing interactions in a self-contained framework. The main contributions are the double-boundary characterization of blind directions (Theorem 3.1), the arithmetic dimension theorem for the standard exchange law (Theorem 4.1), a universal bounded interaction that removes exact blindness on every finite alphabet together with a sharp stability threshold for the standard Hamiltonian (Theorem 5.3 and Propositions 5.4 and 5.5), and the finite-window, calibration and finite-shot analysis of what the restored information costs to read (Sections 6 and 7).

This route also reveals what an observability theorem leaves open. A frequency splitting can remove an exact kernel while leaving the signal too small to measure in a useful time. We retain finite-time conditioning, source-preparation error and sampling noise in the analysis. All numerical examples are calculations of the model. The receiver is tested on fresh source copies, and the reconstructed object is the matched antisymmetric sector, rather than an arbitrary two-mode quantum state.

2 A resonant exchange and its complete receiver channel

2.1 Dynamics and energy accounting

Set $\hbar = 1$. A two-level receiver has states $|d\rangle, |r\rangle$, number operator $N_R = |r\rangle\langle r|$ and energy gap $\varepsilon > 0$. Take positive mode frequencies with $\omega_a - \omega_b = \varepsilon$. The uncoupled

Hamiltonian is

$$H_0 = \varepsilon N_R + \omega_a n_a + \omega_b n_b. \tag{1}$$

For $g > 0$, let

$$V_\psi = g\left(|r\rangle\langle d| \otimes T_\psi + |d\rangle\langle r| \otimes T_\psi^\dagger\right), \tag{2}$$

$$T_\psi = \sum_{n\geq 1, m\geq 0} \psi(n, m+1)|n-1, m+1\rangle\langle n, m|. \tag{3}$$

Here $\psi : \mathbb{N}_0^2 \to [0, \infty)$ is symmetric and $\psi(0, b) = 0$. The dimensionless amplitudes need not be positive in the interior: zero matrix elements will be retained explicitly. Each allowed transition raises the receiver, removes one quantum from mode a and adds one to mode b. Consequently

$$[V_\psi, H_0] = [V_\psi, n_a + N_R] = [V_\psi, n_b - N_R] = 0. \tag{4}$$

On finite-occupation vectors these are direct matrix identities; the block decomposition gives the corresponding commuting spectral evolutions. The gain in uncoupled receiver energy equals the loss in uncoupled source energy. This accounting concerns the closed exchange interval; preparing sources or switching a laboratory device is a separate resource question.

Each state $|d, n, m\rangle$ with $n \geq 1$ belongs to the two-dimensional block spanned by $|d, n, m\rangle$ and $|r, n-1, m+1\rangle$. Dark boundary states complete the decomposition. A finite input alphabet activates only finitely many blocks, including transition partners outside that alphabet. We never turn the input cutoff into a reflecting wall. On the full Fock space, an unbounded interaction is understood through the self-adjoint direct sum of these finite blocks. Boundedness below is a further property, examined in Section 5.3.

The main examples are

$$\psi_0(a, b) = \sqrt{ab}, \qquad \psi_\beta(a, b) = [1 + \beta(a + b - 1)]\sqrt{ab}, \quad \beta \geq 0. \tag{5}$$

Thus $T_0 = ab^\dagger$ and $T_\beta = [1 + \beta(n_a + n_b)]ab^\dagger$. The latter factor changes exchange matrix elements while preserving resonance. Adding a diagonal Kerr term alone would generally change detunings instead; it is not an implementation of Eq. (5).

2.2 Sources matched in their local and thermodynamic data

Let $L \subset \mathbb{N}_0$ contain N occupations and let

$$\rho_S(P) = \sum_{n,m\in L} P_{nm}|n, m\rangle\langle n, m|, \qquad P_{nm} \geq 0, \quad \sum_{nm} P_{nm} = 1. \tag{6}$$

We call the table matched if

$$\sum_m P_{nm} = \sum_m P_{mn} = \pi_n. \tag{7}$$

Then P and P^{T} give the same reduced state on each mode. Transposition permutes their eigenvalues, preserving their entropy and mutual information. Their common mean source energy is $(\omega_a + \omega_b)\sum_n n\pi_n$. Equal spectrum and equal mean energy imply equal ergotropy for the same source Hamiltonian. The distributions of joint source energy need not coincide: because the mode frequencies differ, equality of the mean is the statement used here.

Orient each edge of the complete alphabet graph from i to j for $i < j$. Its incidence matrix D has $+1$ at i and -1 at j. We use J for both the antisymmetric table and its edge-coordinate vector:

$$\begin{gathered} J_{ij} = P_{ij} - P_{ji}, \qquad DJ = 0, \qquad \mathcal{Z}(L) = \ker D, \\ d_N = \dim \mathcal{Z}(L) = \frac{(N-1)(N-2)}{2}. \end{gathered} \tag{8}$$

This is the usual circulation space of a graph [14]. Every direction in it occurs in physical matched sources near a positive product table. In fact, for a real antisymmetric K with $DK = 0$ and strictly positive π,

$$P_{\pm} = \pi\pi^{\mathsf{T}} \pm sK/2 \tag{9}$$

are nonnegative for sufficiently small $|s|$ and satisfy $P_- = P_+^{\mathsf{T}}$. Linear dimension counts therefore describe physically realizable perturbations. They do not supply a probability measure over source tables.

2.3 What the receiver actually measures

Write $x = gt$ and prepare the receiver independently of the source in

$$\rho_R = \begin{pmatrix} 1-q & c \\ \bar{c} & q \end{pmatrix}. \tag{10}$$

The upward and downward transition probabilities are

$$u_{nm}(x) = \sin^2[x\psi(n, m+1)], \qquad d_{nm}(x) = \sin^2[x\psi(n+1, m)]. \tag{11}$$

Define $F_{nm} = u_{nm} - d_{nm}$ and

$$\begin{aligned} S_P(x) &= \sum_{nm} P_{nm}(u_{nm} + d_{nm}), \\ \mathcal{A}_P(x) &= \sum_{nm} P_{nm} F_{nm}(x), \\ C_P(x) &= \sum_{nm} P_{nm} \cos[x\psi(n, m+1)] \cos[x\psi(n+1, m)]. \end{aligned} \tag{12}$$

Tracing the exact Rabi blocks gives, in the interaction picture,

$$q_P = q + (1/2 - q)S_P + \mathcal{A}_P/2, \qquad c_P = cC_P. \tag{13}$$

Symmetry of ψ implies $F_{mn} = -F_{nm}$, and hence

$$S_{P^\intercal} = S_P, \quad C_{P^\intercal} = C_P, \quad \mathcal{A}_{P^\intercal} = -\mathcal{A}_P. \tag{14}$$

The entire difference between the two output states is therefore the population contrast $\mathcal{A}_P$, independently of the receiver input. With $q = 1/2$, the energy changes are $\pm\varepsilon\mathcal{A}_P/2$. For general source pairs, S and C can also change, so the transpose condition is essential to the complete-channel conclusion.

Proposition 2.1 (Single-use distinguishability) *For the channels induced by P and P^{T},*

$$\tfrac{1}{2}\|\Phi_P^x - \Phi_{P^\intercal}^x\|_\diamond = |\mathcal{A}_P(x)|. \tag{15}$$

The equal-prior optimal success probability is $(1 + |\mathcal{A}_P|)/2$. An untouched ancilla offers no improvement.

Proof Linearity of Eq. (13) gives $(\Phi_P^x - \Phi_{P^\intercal}^x)(X) = \mathcal{A}_P \operatorname{Tr}(X) Z_R$, where $Z_R = |r\rangle\langle r| - |d\rangle\langle d|$. On a receiver–ancilla state the output difference is $\mathcal{A}_P Z_R \otimes \rho_{\mathrm{anc}}$, with trace norm $2|\mathcal{A}_P|$. The channel-discrimination characterization of the diamond norm then gives Eq. (15) [15]. Measuring the receiver population already attains the bound. □

3 Two boundaries determine exact blindness

An edge of the occupation graph compares two possible exchanges. Give its endpoints in a second graph the labels

$$\nu_+(i,j) = \psi(i, j+1), \qquad \nu_-(i,j) = \psi(i+1, j), \quad i < j. \tag{16}$$

The vertices of the frequency graph $G_\psi(L)$ are the distinct nonnegative values of these labels. Its incidence map is

$$(B_\psi J)_\nu = \sum_{i<j} J_{ij} \left[\mathbf{1}_{\nu=\nu_+(i,j)} - \mathbf{1}_{\nu=\nu_-(i,j)} \right]. \tag{17}$$

We retain parallel edges and loops; a loop has a zero incidence column. Frequencies denote dimensionless amplitudes here: the cosine angular frequencies in physical time are $2g\nu$.

Theorem 3.1 (Frequency boundary and blind subspace) *For any table P, set $w = B_\psi(P - P^{\mathsf{T}})$. Then*

$$\mathcal{A}_P(x) = -\tfrac{1}{2} \sum_{\nu \geq 0} w_\nu \cos(2\nu x). \tag{18}$$

For matched tables, the exactly blind directions are

$$\mathcal{B}_\psi(L) = \ker D \cap \ker B_\psi. \tag{19}$$

A matched pair induces identical receiver channels at every time, for every receiver input, if and only if its difference lies in this intersection.

Proof Pair the (i,j) and (j,i) entries in Eq. (12). Since $\sin^2 y = (1-\cos 2y)/2$, their contribution is $J_{ij}[\cos(2\nu_- x) - \cos(2\nu_+ x)]/2$. Grouping equal labels proves Eq. (18), including the label zero. Distinct nonnegative-frequency cosines are linearly independent on every open interval. One proof differentiates an identically zero analytic sum at zero: its even derivatives give a Vandermonde system in the distinct numbers ν^2. Thus $\mathcal{A}_P \equiv 0$ exactly when $B_\psi J = 0$. Matching supplies $DJ = 0$, and Eq. (14) gives the channel statement. □

The two kernels have different meanings. The first says that a redistribution leaves local probabilities unchanged. The second says that its positive and negative frequency contributions cancel. Their intersection is the information lost by this interaction. An ideal continuous record on any open interval determines w, or the equivalence class of J in $\mathcal{Z}(L)/\mathcal{B}_\psi(L)$. It does not generally determine P. With several calibrated channels on separately prepared copies, the remaining blind space is $\ker D \cap \bigcap_a \ker B_a$.

3.1 Dark transitions and a possible constant contrast

Zero labels cannot be discarded before their coefficient is known. Let $w_0 = 0$ if zero is absent. The duration-averaged terminal contrast and its squared root-mean-square value are

$$\overline{\mathcal{A}}_P = \lim_{T\to\infty} \frac{1}{T}\int_0^T \mathcal{A}_P(x)\,dx = -\frac{w_0}{2}, \tag{20}$$

$$\nu_P^2 = \lim_{T\to\infty} \frac{1}{T}\int_0^T \mathcal{A}_P(x)^2\,dx = \frac{w_0^2}{4} + \frac{1}{8}\sum_{\nu>0} w_\nu^2. \tag{21}$$

Positive-frequency cosines have zero mean and asymptotically orthogonal products. The zero cosine is constant, giving the different weight in Eq. (21). The centered RMS is $\nu_{c,P}^2 = \sum_{\nu>0} w_\nu^2/8$.

Define an antisymmetric edge function

$$z_{ij} = \mathbf{1}_{\psi(i,j+1)=0} - \mathbf{1}_{\psi(i+1,j)=0}, \qquad i<j. \tag{22}$$

Since $w_0 = z^{\mathsf{T}} J$, the following criterion includes all possible interior dark transitions.

Theorem 3.2 (Neutrality criterion) *Every matched source on L has $\overline{\mathcal{A}}_P = 0$ if and only if*

$$z \in \operatorname{im} D^{\mathsf{T}}. \tag{23}$$

Equivalently, $z_{ij} = h_i - h_j$ for a potential $h : L \to \mathbb{R}$, or the sum of z around every triangle is zero.

Proof All circulation directions are locally physical by Eq. (9). Neutrality for all matched sources is therefore $z^{\mathsf{T}} J = 0$ for every $J \in \ker D$. The finite-dimensional identity $(\ker D)^\perp = \operatorname{im} D^{\mathsf{T}}$ gives Eq. (23). A gradient has zero triangle sums. Conversely, fix an anchor a and set $h_i = z_{ia}$; zero triangle sums imply $z_{ij} = h_i - h_j$. □

Interior positivity,

$$\psi(a,b) > 0 \quad \text{for relevant } a,b \geq 1, \tag{24}$$

is sufficient: $h_i = \mathbf{1}_{i=0}$ gives the required potential. It holds for both amplitudes in Eq. (5). It is not necessary. If $\psi(a,b) = \sqrt{ab}$ when both arguments are odd and is zero otherwise, then $h_i = 1$ on even occupations and zero on odd ones works. There are many dark interior pairs, but every matched source is neutral.

For a contrasting example take $L = \{0,1,2\}$ and $P = (\delta_{01} + \delta_{12} + \delta_{20})/3$, where δ_{ij} is unit mass at table entry (i,j). Keep the standard amplitude except for $\psi(1,1) = 0$. Direct substitution gives

$$\mathcal{A}_P(x) = \tfrac{1}{3}\left[\sin^2(\sqrt{3}x) + \sin^2(\sqrt{2}x) - \sin^2(2x)\right], \qquad \overline{\mathcal{A}}_P = \tfrac{1}{6}, \quad \nu_P^2 = \tfrac{5}{72}. \tag{25}$$

This is a mean over final measurements at different interaction durations. It is not a maintained energy current. The example also shows why conservation and exchange symmetry alone do not imply neutrality.

3.2 An explicit hidden pair

A seven-edge circulation gives a useful benchmark. We embed it in a strictly positive source table for the channel comparisons below. On $L = \{1,2,3,6,7,8\}$ let K be the antisymmetric circulation obtained by adding unit flows around

$$1 \to 8 \to 2 \to 7 \to 1, \qquad 2 \to 3 \to 6 \to 2. \tag{26}$$

For the standard channel the relevant squared labels are

Edge $\{i,j\}$	1,8	2,8	2,7	1,7	2,3	3,6	2,6
$i(j+1)$	9	18	16	8	8	21	14
$(i+1)j$	16	24	21	14	9	24	18

With the signs of K, these edges form one closed frequency cycle, so $DK = B_0 K = 0$. The tables

$$P_\pm = \frac{\mathbf{1}\mathbf{1}^\mathsf{T}}{36} \pm \frac{K}{72} \tag{27}$$

have minimum entry $1/72$, uniform marginals $1/6$ and $P_- = P_+^\mathsf{T}$. Their source trace distance is $7/36$: fourteen ordered entries differ by $1/36$. Their receiver trace distance is exactly zero for every time. The distinction has not disappeared from the source; it has disappeared from this measurement channel.

4 How arithmetic makes the blind space large

This section gives a self-contained bound for the multiplication-table mechanism. For the contiguous alphabet $L_N = \{0,\dots,N-1\}$, the standard squared frequencies are

integers. Let

$$M(N) = |\{ab : 1 \le a, b \le N\}|, \qquad N \ge 3. \tag{28}$$

The positive squared labels appearing on off-diagonal alphabet edges are exactly

$$\{ab : 1 \le a, b \le N\} \setminus \{N(N-1), N^2\}. \tag{29}$$

To verify this, take $1 \le a \le b \le N$. If $b \ge a+2$, use $i(j+1)$ at $(i,j) = (a, b-1)$. If $b = a+1$ and $a \le N-2$, use $(i+1)j$ at $(a-1, a+1)$. If $a = b \le N-1$, use $(a-1, a)$. The only remaining pair labels give the two excluded products; both exceed the largest actual label $(N-1)^2$. Thus there are $m_N = M(N) - 2$ positive frequency coordinates.

Write w_k for the boundary coordinate associated with $\cos(2\sqrt{k}\,x)$; its actual cosine coefficient in $\mathcal{A}_P$ is $-w_k/2$. For a matched standard-channel source,

$$w_0 = 0, \qquad \sum_{k>0} w_k = 0, \qquad \sum_{k>0} k w_k = 0. \tag{30}$$

The first identity follows from interior positivity and matching. The second is the column-sum identity for an incidence matrix. The third follows from

$$\sum_k k w_k = \sum_{i<j} J_{ij}\{i(j+1) - (i+1)j\} = \sum_i i \sum_j J_{ij} = 0. \tag{31}$$

The last two restrictions are independent because there is more than one distinct positive label.

Theorem 4.1 (Dimension of arithmetic blindness) *Let* $r_N = \operatorname{rank}(B_0|_{\mathcal{Z}(L_N)})$ *and* $d_N = (N-1)(N-2)/2$. *Then*

$$r_N \le \min\{d_N, M(N) - 4\}, \tag{32}$$

$$\frac{\dim \mathcal{B}_0(L_N)}{d_N} \ge \max\left\{0, 1 - \frac{2[M(N)-4]}{(N-1)(N-2)}\right\} \longrightarrow 1. \tag{33}$$

More precisely, with $\delta = 1 - (1 + \log\log 2)/\log 2 = 0.08607\ldots$,

$$\frac{r_N}{d_N} = O\left((\log N)^{-\delta}(\log\log N)^{-3/2}\right). \tag{34}$$

Proof There are $M(N)-2$ positive coordinates and two independent linear constraints, proving Eq. (32). Rank–nullity gives Eq. (33). The multiplication-table problem goes back to Erdős [16]. Ford's sharp theorem gives $M(N) \asymp N^2(\log N)^{-\delta}(\log\log N)^{-3/2}$ [17]; substitution yields Eq. (34). □

The asymptotic statement is about dimension, not typicality. At any fixed size with a nonzero visible sector, a proper blind subspace still has zero volume under a nonsingular continuous distribution on all circulation directions. What grows to one is its fraction of the available linear dimensions. Nor is the rank bound asserted to be sharp. The exact calculations show both points clearly.

Table 1 Standard-channel ranks calculated over the rationals. The fourth column is the bound in Eq. (32); the blind fraction is exact nullity divided by d_N.

N	d_N	r_N	Rank bound	Nullity	Blind fraction
8	21	21	21	0	0.0000
9	28	26	28	2	0.0714
10	36	32	36	4	0.1111
12	55	49	55	6	0.1091
16	105	85	93	20	0.1905
20	171	138	148	33	0.1930
30	406	292	304	114	0.2808
40	741	498	513	243	0.3279

Direct integer counting gives $M(100) = 2906$ and $M(1000) = 248083$. The corresponding lower bounds on the blind fraction are $1949/4851 = 0.4017728\ldots$ and $83474/166167 = 0.5023500454\ldots$. These are counting bounds; they are not extrapolated exact ranks. Finite-size fractions need not be monotone, as Table 1 illustrates.

4.1 Why the first contrast is fourth order

The two sum rules also have a dynamical meaning. The response starts from zero, and its quadratic term vanishes. Expanding the standard transition probabilities gives

$$\mathcal{A}_P(x) = -\frac{2x^4}{3} \sum_{nm} P_{nm} nm(n-m) + O_L(x^6). \tag{35}$$

Indeed, the quadratic difference is $n-m$ and the quartic difference is $2nm(n-m)+n^2-m^2$; matching cancels the single-occupation terms. For the three-cycle $0 \to 1 \to 2 \to 0$ with equal weights, the remaining coefficient is $4/9$. Some sources cancel further orders, and blind sources cancel all of them.

There is a finite exact stopping rule. If $m = m_N$ positive labels are used, then

$$\mathcal{A}_P^{(2s)}(0) = (-1)^{s+1} 2^{2s-1} \sum_{k>0} k^s w_k. \tag{36}$$

The known zero moments $s = 0, 1$, together with derivatives of orders $4, 6, \ldots, 2(m-1)$, determine w by an invertible Vandermonde matrix. A nonzero standard-channel contrast therefore has an onset between orders 4 and $2(m-1)$. This is an exact algebraic certificate; estimating high derivatives from noisy data would usually be a poor reconstruction method.

5 Removing blindness without losing a stable Hamiltonian

5.1 The graph before numerical labels are merged

Before assigning a frequency, retain the unordered pair $\{a, b\}$ itself as a vertex. Each alphabet edge $\{i, j\}$ joins $\{i, j+1\}$ to $\{i+1, j\}$. Call this the pair graph. Its edge preserves the sum $s = i+j+1$. For a fixed s, ordering pairs $\{a, s-a\}$ by their smaller member shows that an edge connects consecutive values. Each component is a path, and different sums remain separate.

Theorem 5.1 (A sufficient separation criterion) *Suppose ψ is positive and injective on the positive unordered pair labels appearing in the pair graph. Then the frequency graph is a forest and $\mathcal{B}_\psi(L) = \{0\}$.*

Proof Injectivity leaves the positive pair vertices distinct. Mandatory zero vertices $\{0, s\}$ are leaves, with at most one in each component. Identifying one leaf from each of several disjoint trees cannot create a cycle. The resulting graph remains a forest, whose incidence matrix has zero edge kernel. Equation (19) then proves the claim. □

A frequency collision is not by itself evidence for a blind matched source. It must create a frequency circulation that also has zero occupation boundary. This distinction matters when a single positive pair is assigned amplitude zero. If all positive pair labels remain mutually distinct, at most one can be zero. Merging that vertex with the common zero vertex creates at most one frequency cycle. If a cycle is created, it contains exactly one alphabet edge incident to occupation zero, so its occupation boundary is nonzero. Thus $\mathcal{B}_\psi(L)$ still vanishes even though the frequency graph may no longer be a forest. The complete argument is given in the accompanying methods document.

Proposition 5.2 (What scalar relabelling cannot change) *If $\widetilde{\psi} = h \circ \psi$ with $h \geq 0$ and $h(0) = 0$, then $\mathcal{B}_\psi(L) \subseteq \mathcal{B}_{\widetilde{\psi}}(L)$. Equality holds if h is injective on the used labels.*

Proof The new boundary sums old coefficients over the frequency labels merged by h. Hence $B_{\widetilde{\psi}} = R_h B_\psi$ for a coordinate-merging map R_h. An injective relabelling just reindexes the coefficients. □

In particular, rescaling g cannot repair exact blindness. A scalar envelope multiplying the same fixed V_ψ changes only the accumulated interaction time because the Hamiltonians commute at different times. For that control class, one must change the frequency identifications themselves. Noncommuting receiver controls are a different measurement model.

5.2 One algebraic coefficient separates every finite alphabet

Theorem 5.3 (Universal pair separation) *For a fixed finite alphabet, all but finitely many $\beta \geq 0$ in Eq. (5) separate its positive pair labels. Any positive algebraic β of degree greater than two separates all positive unordered integer pairs. In particular,*

$$\beta_* = \sqrt[3]{2}/20 = 0.06299605249\ldots \tag{37}$$

gives $\mathcal{B}_{\psi_{\beta_*}}(L) = \{0\}$ for every finite L.

Proof Put $k = ab$ and $s = a + b - 1$. A collision is $(1 + s\beta)\sqrt{k} = (1 + s'\beta)\sqrt{k'}$. For different unordered pairs this is a nonzero affine equation in β: equal constant and linear coefficients would give $k = k'$ and $s = s'$, which determine the same pair. Finitely many pairs thus have only finitely many exceptional coefficients. Squaring a collision yields

$$(ks^2 - k's'^2)\beta^2 + 2(ks - k's')\beta + (k - k') = 0. \tag{38}$$

The polynomial is nonzero and has integer coefficients. An algebraic number of degree greater than two cannot satisfy it. The value in Eq. (37) has degree three, with minimal polynomial $4000z^3 - 1$. Positivity and Theorem 5.1 finish the proof. □

The same coefficient works across finite cutoffs; it is not fitted separately at each N. This does not demand an infinitely precise experimental dial. On a specified finite alphabet, let Δ_L be the minimum separation in the set consisting of zero and all distinct positive used amplitude values, whether or not zero occurs in the original frequency graph. Suppose the calibrated amplitude remains symmetric, nonnegative and zero on the mandatory boundary. If every unordered-pair amplitude changes by at most $\eta < \Delta_L/2$, distinct nominal labels remain distinct and positive labels remain positive. Pair separation, and therefore identifiability, survives. No uniform gap as L grows is claimed.

5.3 The energy lower bound deserves its own check

Commuting with H_0 ensures conservation, but it does not ensure that $H_0 + V_\psi$ has a lower energy bound. The distinction is already present in the standard channel.

Proposition 5.4 (Sharp standard-channel stability threshold) *For $\omega_a, \omega_b > 0$, the full direct-sum Hamiltonian with $\psi_0(a, b) = \sqrt{ab}$ is bounded below if and only if*

$$g \leq 2\sqrt{\omega_a \omega_b}. \tag{39}$$

For every $\beta > 0$, the raw dressed Hamiltonian in Eq. (5) is unbounded below on unrestricted Fock space.

Proof Write $a = n \geq 1$ and $b = m + 1 \geq 1$. The two basis states of a resonant block have common free energy $E_{ab} = \omega_a a + \omega_b b - \omega_b$. Its lower standard eigenvalue is

$$E^-_{ab} = \omega_a a + \omega_b b - \omega_b - g\sqrt{ab}. \tag{40}$$

At or below Eq. (39), the arithmetic–geometric mean inequality gives $E^-_{ab} \geq -\omega_b$. The uncoupled boundary energies are nonnegative. Above the threshold, choose a positive rational

ratio a/b close enough to ω_b/ω_a that $\omega_a a + \omega_b b - g\sqrt{ab} < 0$. Scaling that integer pair sends E^-_{ab} to $-\infty$. For the raw dressing, choosing $a = b = n$ gives $E^-_{nn} = (\omega_a + \omega_b)n - \omega_b - g[1 + \beta(2n-1)]n \to -\infty$. □

Finite occupied blocks still have exact, finite-dimensional unitary dynamics in both cases. The full-space threshold is needed when those blocks are promoted to a global model. At the critical threshold we use the natural direct-sum domain; we do not identify it with the domain of H_0.

Proposition 5.5 (Bounded observing interaction) *Define*

$$\widehat{\psi}_*(a,b) = \frac{\psi_{\beta_*}(a,b)}{1 + \psi_{\beta_*}(a,b)}. \tag{41}$$

This amplitude has no blind matched direction on any finite alphabet. Its full Hamiltonian is self-adjoint on $D(H_0)$ and satisfies $H_0 + V_{\widehat{\psi}_*} \geq -gI$.

Proof The function $h(y) = y/(1+y)$ is strictly increasing on $[0,\infty)$ and fixes zero. It preserves the frequency identification pattern, so Proposition 5.2 and Theorem 5.3 preserve identifiability. Each exchange block now has amplitude below one, giving $\|V_{\widehat{\psi}_*}\| \leq g$. The bounded-perturbation theorem gives self-adjointness on $D(H_0)$ [18]; $H_0 \geq 0$ gives the lower bound. □

Equation (41) is an existence construction for a stable, information-resolving interaction. Its compressed high-occupation frequencies may be difficult to resolve in time. This is why the finite-window analysis and the equal-peak comparison below are needed alongside the exact theorem.

6 Exact access and useful sensitivity are different

6.1 Finite-time Gramian and calibration error

The frequency boundary determines what can be learned in principle. To ask how well it can be learned in a finite window, put $c_\nu(x) = -\cos(2\nu x)/2$ and include zero if it occurs. Direct integration gives

$$G_T(\nu,\nu') = \frac{1}{8}\left\{\operatorname{sinc}[2T(\nu-\nu')] + \operatorname{sinc}[2T(\nu+\nu')]\right\}, \qquad \operatorname{sinc} z = \frac{\sin z}{z}, \quad \operatorname{sinc} 0 = 1. \tag{42}$$

Let Q have orthonormal columns spanning $\mathcal{Z}(L)$ in edge coordinates and define

$$W_\psi(T) = Q^{\mathsf{T}} B_\psi^{\mathsf{T}} G_T B_\psi Q. \tag{43}$$

For $J = Qv$, the quadratic form $v^{\mathsf{T}} W_\psi(T) v$ equals $T^{-1}\int_0^T \mathcal{A}_J(x)^2\,dx$. Its kernel is the blind space for every $T > 0$: a nonnegative continuous square has zero integral precisely when the analytic response vanishes throughout the interval. Small nonzero

eigenvalues instead describe weakly observed directions. This is the finite-record version of the observability distinction in dynamical tomography [19, 20]; the explicit incidence matrix supplies the model-specific reduction.

Suppose both endpoint amplitudes of every edge change by at most η. The function $\sin^2 y$ is one-Lipschitz. For a physical source that was blind before the perturbation,

$$|\widetilde{\mathcal{A}}_P(x)| \le \min\{1, 2|x|\eta\}\|J\|_{1,E}, \qquad \|J\|_{1,E} = \sum_{i<j} |J_{ij}| \le 1. \tag{44}$$

For a unit edge-coordinate vector, $\|J\|_{1,E} \le \sqrt{E}$ with $E = \binom{N}{2}$. If the original blind space has dimension b, the min–max principle therefore places at least b eigenvalues of the perturbed Gramian below or at

$$\frac{4E\eta^2T^2}{3}. \tag{45}$$

A rank jump can be discontinuous even when every accessible finite-window signal changes continuously. The smallest frequency gap gives a useful calibration scale, but the singular values of the actual measurement design determine statistical stability. This separation between uniqueness and stable recovery also appears in spectral super-resolution [21, 22]; its constants are not imported into our cosine model.

6.2 Time averages, marginal spread and source optimization

The distinction between a small signed mean and a small fluctuation is familiar in finite-time equilibration [23]. Here both quantities are explicit. With $\nu_{\min}$ the smallest positive label,

$$\left| \frac{1}{T}\int_0^T \mathcal{A}_P(x)\,dx - \overline{\mathcal{A}}_P \right| \le \frac{1}{4T}\sum_{\nu>0}\frac{|w_\nu|}{\nu} \le \frac{\|J\|_{1,E}}{2T\nu_{\min}}. \tag{46}$$

If there is no positive label, the centered response is zero. For the standard contiguous alphabet, $\nu_{\min} = 1$ and the mean is zero, so Eq. (46) is at most $1/(2T)$. The RMS need not decay with elapsed time.

Let Δ_+ be the largest absolute row sum of the positive-frequency incidence matrix, with loop columns cancelled. Since $|J_{ij}| \le \min(\pi_i, \pi_j)$ and $\|w_+\|_1 \le 2$, Eq. (21) gives

$$\nu_{c,P} \le \tfrac{1}{2}\sqrt{\Delta_+\pi_{\max}}, \qquad \pi_{\max} = \max_i \pi_i. \tag{47}$$

For the standard channel, the number of incidences at a squared label k is at most the number of positive divisors of k. The classical subpower divisor bound gives $\Delta_+ = N^{o(1)}$ [24]. With uniform marginals, Eq. (47) is therefore bounded above by $N^{-1/2+o(1)}$. It is an upper bound on RMS, not an asymptotic equality for each source. Spreading the marginal is essential: embedding a fixed three-occupation cycle in a larger alphabet leaves its RMS unchanged.

For uniform marginals, NP is doubly stochastic. Birkhoff's decomposition into permutation matrices [25] turns the instantaneous optimization into an assignment problem:

$$R_N(x) = \max_P \mathcal{A}_P(x) = \frac{1}{N} \max_{\sigma \in S_N} \sum_i F_{i,\sigma(i)}(x). \tag{48}$$

This is the classical linear assignment problem [26]. The optimizing source can change with time. The RMS is a norm of a linear function of P, so convexity also puts at least one RMS maximizer at a permutation source. Exhaustive enumeration can therefore certify the finite-size optimum. Finally, $|\sin^2 y - y^2| \le y^4/3$ and the quadratic cancellation give the uniform early-time bound

$$R_N(x) \le \min\{1, \tfrac{2}{3}(N-1)^4 x^4\}. \tag{49}$$

No finite alphabet gives an order-one optimized contrast at all prescribed times, including times arbitrarily close to zero.

6.3 A finite-shot decision rule

Choose L_t channel–time settings before acquiring outcomes. At each setting, prepare S independent copies of P and S of P^{T} and measure the final receiver population. Let $\widehat{\mathcal{A}}_\ell$ be the difference of the two empirical excitation frequencies. Hoeffding's inequality applied directly to the $2S$ weighted Bernoulli variables, followed by a union bound [27], gives

$$\Pr\left[\max_\ell |\widehat{\mathcal{A}}_\ell - \mathcal{A}_\ell^{\text{actual}}| > \eta_S\right] \le \alpha, \qquad \eta_S = \sqrt{\frac{\log(2L_t/\alpha)}{S}}. \tag{50}$$

If the actual expected contrast differs from the nominal model by at most a separately established δ_{tot} at every setting, the simultaneous model-error radius is $e = \eta_S + \delta_{\text{tot}}$. Under a nominally blind hypothesis, the rule $|\widehat{\mathcal{A}}_\ell| > e$ has familywise false-positive probability at most α. A specified alternative with $|\mathcal{A}_\ell| > 2e$ is detected on the same coverage event, giving detection probability at least $1 - \alpha$ under the stated independent-shot model. The systematic error budget must be justified by calibration; increasing S cannot remove it.

For a fixed channel, one can also reconstruct the visible coefficients. Let U have orthonormal columns spanning $B_\psi \mathcal{Z}(L)$, write $w = U\theta$, and set $C_{\ell\nu} = -\cos(2\nu x_\ell)/2$. If $H = CU$ has full column rank, least squares obeys

$$\|\widehat{\theta} - \theta\|_2 \le \frac{\sqrt{L_t}(\eta_S + \delta_{\text{tot}})}{\sigma_{\min}(H)}. \tag{51}$$

Full rank is a starting point; the denominator determines whether the estimate is useful. To transfer this estimate to circulation coordinates, one also needs the inverse singular values of the restricted boundary map. A two-setting witness test is not a reconstruction of every coefficient.

A practical experiment would use Eq. (27) in two stages. The standard interaction predicts no contrast; the calibrated dressing predicts one. The first stage should report an upper confidence bound, rather than treat a nonsignificant test as proof of exact blindness. The second should resolve the predicted contrast within a controlled preparation, timing, matrix-element and readout budget. Coupled-mode experiments already demonstrate coherent exchange processes [28], but implementing the specific amplitude law, while maintaining exchange symmetry and resonance, remains a separate engineering task. Any derivation through an eliminated intermediate level also needs a controlled approximation and its associated detuning corrections [29].

7 Reproducible calculations and a fair channel comparison

The accompanying code reconstructs the model from occupation transitions, regenerates the figures and writes machine-readable results. Exact identities use integers or rational arithmetic. Floating-point propagation tests the implementation against the analytic formulas. The fixed random seed is 20261030; library versions, individual checks and numerical errors are recorded in `results/results.json` and `results/test_log.json`. The methods document gives the executable commands and the scope of each test.

7.1 Exact ranks and physical sources

The rational rank calculation uses anchored triangles $0 \to i \to j \to 0$. Their standard frequency boundaries are

$$-\delta_i + \delta_j + \delta_{i(j+1)} - \delta_{(i+1)j}, \qquad 1 \le i < j \le N-1, \tag{52}$$

where repeated squared labels are combined before elimination. Ranks were calculated for $N = 3, \ldots, 12, 16, 20, 30, 40$. The package records an exact kernel basis at $N = 9$. Integer product sets supply the larger-size bounds in Figure 1.

All 409110 permutation sources for $3 \le N \le 9$ were enumerated. The maximal squared RMS values are, respectively,

$$\frac{1}{18}, \frac{1}{16}, \frac{7}{100}, \frac{1}{16}, \frac{3}{49}, \frac{7}{128}, \frac{5}{81}. \tag{53}$$

A second implementation based on rational fractions independently reproduced these optima and the ranks through $N = 12$. Both versions test the same mathematical model; this is an implementation cross-check, not external experimental replication.

7.2 Full Hamiltonian and channel checks

For the hidden pair, ten Fock levels per mode include every occupied state and every exchange partner. The resulting receiver–mode matrix is 200×200. With $\varepsilon = 1, \omega_a = 3$, $\omega_b = 2$ and $g = 1$, its interaction-picture unitary was compared with Eq. (13) at 41

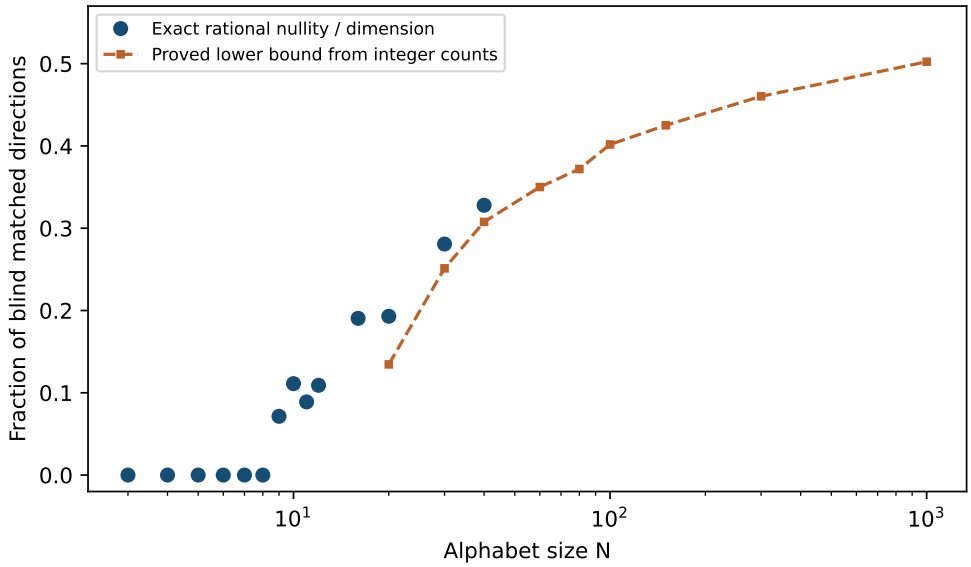


Fig. 1 Blind dimensions for the standard exchange law. Rational elimination gives the displayed exact ratios; larger-size values are proved lower bounds obtained by counting distinct integer products. The two series are not interchangeable.

times in $[0, 10]$, for each source and each of the standard, raw cubic and bounded cubic amplitudes. The receiver input had $q = 0.3$ and $c = 0.4$. The maximum entrywise reduced-state discrepancy was below 9×10^{-16}; the trace-distance identity differed by less than 5×10^{-16}. The constructed conservation commutators were zero.

Additional tests cover 100 receiver–ancilla states with ancilla dimension three, 100 coefficient-Gramian entries against adaptive quadrature, 100 frequency-perturbation cases at 101 times each, and 105 single-interior-zero graph cases. The dark-transition example gives $w_0 = -1/3$, mean $1/6$ and squared RMS $5/72$ exactly. For cubic separation, the finite graph uses the exact unordered pair label justified by Theorem 5.3; numerical equality tests are not used to certify the irrational-frequency theorem.

7.3 The cost of bounded amplitudes at equal peak coupling

An unscaled comparison would be misleading: the raw cubic amplitude reaches 17.0379091 on the fully populated support of Eq. (27), whereas the bounded amplitude reaches 0.9445612. We therefore divide each law by its maximum over both receiver transitions from every initially populated $(n, m) \in L \times L$. Both normalized channels then have maximum amplitude one on this common support and share the same g. This is a finite-support peak constraint; it does not claim equal implementation cost or equal global operator norms.

Both channels remain injective on the matched sector. For this witness they also have the same exact infinite-time squared RMS, $1/1296$: injective relabelling leaves the eight nonzero boundary coefficients, each of magnitude $1/36$, unchanged. Their finite-window sensitivities are very different. The smallest gaps between positive labels are

Table 2 Numerical finite-window sensitivity at equal support peak amplitude. Gain is $\sqrt{\lambda_{\min}(W(T))}$ in orthonormal edge coordinates. The condition number shown is the ratio of largest to smallest gains, not the squared Gramian condition number. Values come from positive-weight time quadrature and singular-value decomposition.

Channel	T	Minimum gain	Gain condition number
Raw cubic, normalized	50	0.114674	6.418
Bounded cubic, normalized	50	0.000175359	4097.668
Raw cubic, normalized	300	0.299183	2.052
Bounded cubic, normalized	300	0.142861	4.707

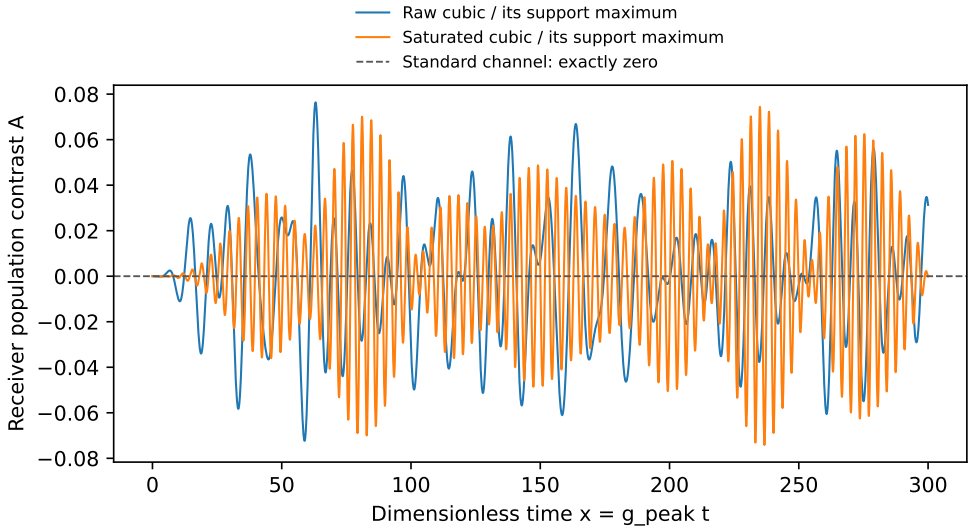


Fig. 2 The strictly positive hidden pair under standard and dressed interactions, with dressed channels normalized to the same peak amplitude on the full populated support. The standard response is exactly zero. Time is measured in units of g^{-1}. Displayed extrema are finite-grid values, not certified continuous-time maxima.

approximately 0.0054660 for the normalized raw law and 0.00047466 for the normalized bounded law. Table 2 compares all ten matched directions on the six-occupation alphabet, rather than only the chosen witness.

On the common grid $x \in [0, 300]$ with spacing 0.015, the normalized raw channel reaches $|\mathcal{A}| = 0.0763916$ at $x = 63.075$, while the normalized bounded channel reaches 0.0744151 at $x = 234.945$. These are grid extrema. Saturation has preserved exact access and long-time RMS, but compresses frequencies enough to postpone a useful record. No universal performance ordering is inferred from this example.

For a concrete planning calculation, fix the bounded-channel setting at $x = 234.945$ before collecting data, together with one standard-channel control. With $L_t = 2$, $\alpha =$

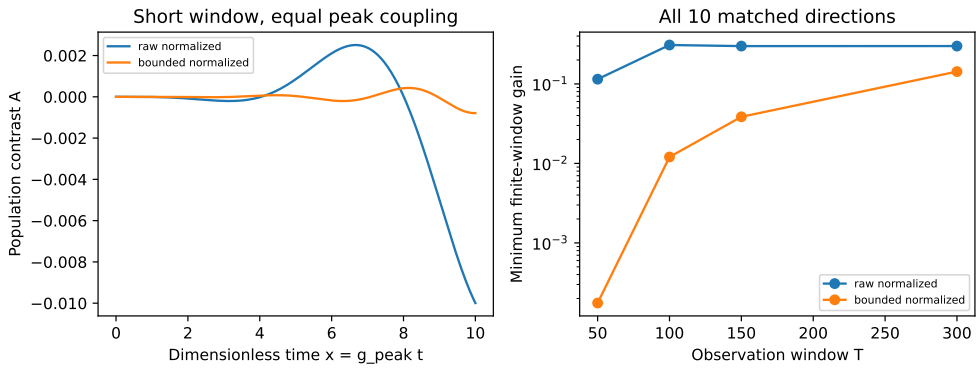


Fig. 3 Conditioning on the full matched circulation space for the same equal-peak comparison. Extending the window greatly improves the bounded channel's sensitivity. Exact injectivity alone does not specify this time cost. Numerical near-zero singular values at short windows should not be read as additional exact kernels.

0.01 and $S = 15000$ shots per source per setting, Eq. (50) gives $\eta_S = 0.019986$. If calibration establishes $\delta_{\mathrm{tot}} \leq 0.01$, the predicted contrast exceeds $2(\eta_S + \delta_{\mathrm{tot}}) = 0.059972$. The decision rule in Section 6.3 then has the stated 99% simultaneous coverage and conditional detection guarantee. This plan uses 60000 source preparations in total; the systematic budget is a required condition, not a measured property of a device.

8 Discussion

The calculation starts from a distinction that thermodynamic summaries do not settle: having correlations and being able to read them are different questions. Equal marginals, spectrum and ergotropy leave a large family of matched sources. A fixed receiver sees only their frequency boundary. For the standard interaction, multiplication-table coincidences reduce the accessible dimension so severely that the blind fraction tends to one. A bounded interaction satisfying the same resonance and conservation relations can remove that exact loss on every finite alphabet.

The result sits within quantum observability, rather than replacing it. Recent work shows how a single evolving expectation can identify states under suitable dynamical assumptions, and how Krylov spaces organize reconstructible subspaces [19, 20]. Designed measurement sequences provide a complementary route to tomography [30]. Here the restricted source family and exactly solvable exchange turn that general question into an explicit arithmetic graph problem. Number-diagonal sources are separable and can be distinguished by correlated number measurements; their invisibility is a property of the stipulated receiver channel, not a form of entanglement-based data hiding.

Several extensions are worth pursuing. A physically realizable amplitude should be optimized for minimum singular value under a specified control budget, rather than chosen only for algebraic injectivity. Detuning, loss and coherent source components would change the response basis and must be included in their own calibrated models. Several simple exchange laws may prove more practical than one universally

separating law, because their combined blind spaces can shrink without requiring a large nonlinear dressing. The present graph maps provide a direct way to evaluate that trade-off.

The main lesson is operational. Exact blindness is a cancellation that time cannot repair. Removing the cancellation requires a different interaction, and making the recovered information useful requires adequate frequency resolution, preparation accuracy and statistical precision. The double-boundary criterion, stability classification and finite-shot certificate make those three requirements separately calculable.

Declarations

Author contribution. Ahmet Faruk Arapoğlu formulated the research question, performed the analysis and wrote the manuscript, and is the sole author.

Use of generative artificial intelligence. ChatGPT versions 5.6 and 6.0 were used for mathematical calculations, literature searches, translation, restructuring, language editing and manuscript formatting. The author takes full responsibility for the scientific reasoning, derivations, computational results and final text.

Funding and competing interests. No external funding was received. The author declares no competing interests.

Data and code availability. The accompanying electronic supplement contains the Python source, exact source tables, numerical results, figures, environment requirements and instructions needed to reproduce the reported calculations. No experimental dataset is used.

References

[1] M. Perarnau-Llobet, K. V. Hovhannisyan, M. Huber, P. Skrzypczyk, N. Brunner and A. Acín: Extractable work from correlations. Phys. Rev. X **5**, 041011 (2015). https://doi.org/10.1103/PhysRevX.5.041011

[2] K. Micadei et al.: Reversing the direction of heat flow using quantum correlations. Nat. Commun. **10**, 2456 (2019). https://doi.org/10.1038/s41467-019-10333-7

[3] R. P. A. Simon, J. Anders and K. V. Hovhannisyan: Correlations enable lossless ergotropy transport. Phys. Rev. Lett. **134**, 010408 (2025). https://doi.org/10.1103/PhysRevLett.134.010408

[4] A. E. Allahverdyan, R. Balian and Th. M. Nieuwenhuizen: Maximal work extraction from finite quantum systems. Europhys. Lett. **67**, 565–571 (2004). https://doi.org/10.1209/epl/i2004-10101-2

[5] A. Jamiołkowski: Minimal number of operators for observability of N-level quantum systems. Int. J. Theor. Phys. **22**, 369–376 (1983). https://doi.org/10.1007/BF02082903

[6] D. D'Alessandro: On quantum state observability and measurement. J. Phys. A: Math. Gen. **36**, 9721–9735 (2003). https://doi.org/10.1088/0305-4470/36/37/310

[7] D. D'Alessandro and R. Romano: Further results on the observability of quantum systems under general measurement. Quantum Inf. Process. **5**, 139–160 (2006). https://doi.org/10.1007/s11128-006-0022-5

[8] M. Kech: Dynamical quantum tomography. J. Math. Phys. **57**, 122201 (2016). https://doi.org/10.1063/1.4968816

[9] B. M. Terhal, D. P. DiVincenzo and D. W. Leung: Hiding bits in Bell states. Phys. Rev. Lett. **86**, 5807–5810 (2001). https://doi.org/10.1103/PhysRevLett.86.5807

[10] D. P. DiVincenzo, D. W. Leung and B. M. Terhal: Quantum data hiding. IEEE Trans. Inf. Theory **48**, 580–598 (2002). https://doi.org/10.1109/18.985948

[11] B. Buck and C. V. Sukumar: Exactly soluble model of atom-phonon coupling showing periodic decay and revival. Phys. Lett. A **81**, 132–135 (1981). https://doi.org/10.1016/0375-9601(81)90042-6

[12] C. C. Gerry and J. H. Eberly: Dynamics of a Raman coupled model interacting with two quantized cavity fields. Phys. Rev. A **42**, 6805–6815 (1990). https://doi.org/10.1103/PhysRevA.42.6805

[13] X. Yang, Y. Wu and Y. Li: Unified and standardized procedure to solve various nonlinear Jaynes–Cummings models. Phys. Rev. A **55**, 4545 (1997). https://doi.org/10.1103/PhysRevA.55.4545

[14] J. A. Bondy and U. S. R. Murty: Graph Theory. Graduate Texts in Mathematics, vol. 244. Springer, London (2008). https://doi.org/10.1007/978-1-84628-970-5

[15] J. Watrous: The Theory of Quantum Information. Cambridge University Press, Cambridge (2018). https://doi.org/10.1017/9781316848142

[16] P. Erdős: An asymptotic inequality in the theory of numbers (in Russian). Vestnik Leningrad. Univ. **15**, 41–49 (1960).

[17] K. Ford: The distribution of integers with a divisor in a given interval. Ann. Math. **168**, 367–433 (2008). https://doi.org/10.4007/annals.2008.168.367

[18] M. Reed and B. Simon: Methods of Modern Mathematical Physics, vol. I: Functional Analysis. Academic Press, New York (1972). https://doi.org/10.1016/B978-0-12-585001-8.X5001-6

[19] H. Rall and M. M. Wolf: Quantum tomography from the evolution of a single expectation. Ann. Henri Poincaré **27**, 2939–2962 (2026). https://doi.org/10.1007/s00023-025-01617-4

[20] M. Peruzzo, T. Grigoletto and F. Ticozzi: Reconstructing quantum states and expectations via dynamical tomography. Phys. Rev. A **113**, 032435 (2026). https://doi.org/10.1103/x88t-j8k9

[21] A. Moitra: Super-resolution, extremal functions and the condition number of Vandermonde matrices. In: Proceedings of the 47th Annual ACM Symposium on Theory of Computing, pp. 821–830. ACM, New York (2015). https://doi.org/10.1145/2746539.2746561

[22] E. J. Candès and C. Fernandez-Granda: Towards a mathematical theory of super-resolution. Commun. Pure Appl. Math. **67**, 906–956 (2014). https://doi.org/10.1002/cpa.21455

[23] A. J. Short and T. C. Farrelly: Quantum equilibration in finite time. New J. Phys. **14**, 013063 (2012). https://doi.org/10.1088/1367-2630/14/1/013063

[24] G. H. Hardy and E. M. Wright: An Introduction to the Theory of Numbers, 6th edn. Oxford University Press, Oxford (2008). https://doi.org/10.1093/oso/9780199219858.001.0001

[25] G. Birkhoff: Tres observaciones sobre el álgebra lineal. Univ. Nac. Tucumán Rev. Ser. A **5**, 147–151 (1946).

[26] H. W. Kuhn: The Hungarian method for the assignment problem. Nav. Res. Logist. Q. **2**, 83–97 (1955). https://doi.org/10.1002/nav.3800020109

[27] W. Hoeffding: Probability inequalities for sums of bounded random variables. J. Am. Stat. Assoc. **58**, 13–30 (1963). https://doi.org/10.1080/01621459.1963.10500830

[28] G. Maslennikov, S. Ding, R. Hablützel, J. Gan, A. Roulet, S. Nimmrichter, J. Dai, V. Scarani and D. Matsukevich: Quantum absorption refrigerator with trapped ions. Nat. Commun. **10**, 202 (2019). https://doi.org/10.1038/s41467-018-08090-0

[29] E. Brion, L. H. Pedersen and K. Mølmer: Adiabatic elimination in a lambda system. J. Phys. A: Math. Theor. **40**, 1033–1043 (2007). https://doi.org/10.1088/1751-8113/40/5/011

[30] V. Gonzalez Avella, J. Czartowski, D. Goyeneche and K. Życzkowski: Cyclic measurements and simplified quantum state tomography. Quantum **9**, 1763 (2025). https://doi.org/10.22331/q-2025-06-04-1763

Supplementary Files

This is a list of supplementary files associated with this preprint. Click to download.

- ArithmeticBlindnessMethodsEN.pdf
- QIPComputationalSupplement.zip